Computation of Time-Resolved EPR Spectra of Systems Exhibiting Electron Spin Polarization Complicated by Magnetization Transfer

Martin Jäger and James R. Norris, Jr.*,†

Department of Chemistry, University of Chicago, 5735 South Ellis Avenue, Chicago, Illinois 60637

Received: September 13, 2001

In order that chemically induced dynamic electron polarization (CIDEP) can provide a means to explore dynamics in arbitrary systems such as inclusion compounds or sequential chemical reactions, the Bloch equations are extended for use with a system exhibiting electron spin polarization (ESP). Since CIDEP depends on time and external magnetic field and in this paper is observed by time-resolved electron paramagnetic resonance spectroscopy (TREPR), an algorithm for the general calculation of EPR signals that display ESP is presented. In particular, processes inducing magnetization transfer between hyperfine (hf) states are described by means of a kinetic matrix that is incorporated into the Bloch relaxation matrix. The utilized approach takes into account the complete set of hyperfine states of all involved species and can be applied to such different phenomena as chemical exchange, electron transfer, and secondary radical generation that affect the time dependence of the observed signal. Solutions to the linear differential equations are found numerically. Hence, other than the normal restrictions on the Bloch equations, no additional approximations are assumed, rendering the algorithm more generally applicable than previous analytical treatments. Only chemical diffusion is not included. Specific examples are discussed. The TREPR spectra of *p*-benzoquinone are analyzed in terms of magnetization transfer. Excellent agreement between the experimental data and the computations using the numerical method is achieved. With rate constants depending on pH and solvent, chemical exchange between the neutral and/or anionic semiquinones is found present in the signals of the radicals generated by laser flash photolysis.

Introduction

Chemically induced dynamic electron polarization (CIDEP) and the more general electron spin polarization (ESP) are well-understood phenomena.[13,16−18,26] The description of the quantities observed in time-resolved electron paramagnetic resonance (TREPR) experiments, i.e., the *y*-magnetization of paramagnetic species after photolysis, has been extensively discussed by several authors.[5,20,24,25] The common approach is based upon a Bloch equation treatment where, according to the experimental conditions, modifications are applied to the original differential equations in order to include or exclude radical termination reactions, F-pair polarization, secondary radical generation, etc. Only a few, albeit thorough, attempts have been performed to introduce chemical exchange and electron transfer into the model and analyze their effects on the EPR signals simultaneously in the field and time domains.[6,14,15] These pioneering efforts by necessity focused on systems with well-defined, spin dynamics simple enough to obey the computational and mathematical analytical restrictions when simulating EPR spectral results. For CIDEP and ESP to achieve full impact in chemical applications, the choice of spin systems as a probe will have to satisfy chemical requirements rather than theoretical implications. Thus systems are likely to exhibit complicated ESP patterns that will require more complex spectral simulations.

In this report, we will present a generalized algorithm for the computation of TREPR spectra of ESP systems. This more extensive approach includes such effects as chemical exchange, electron transfer (ET), and secondary radicals without specific limitations to experimental conditions. The formalism of the method permits CIDEP and ESP to be used as a tool for the examination of rather complicated spin systems, for example, zeolites,[8] fullerenes and their adducts,[9] cyclodextrins,[23] micelles,[11,12] and even "simple" biochemical compounds.[19] We will apply a complete matrix treatment where the solution of the modified Bloch equations is traced back to an eigenvalue problem, which is well suited for use with today's fast computer technology. The treatment considers all magnetic resonance and kinetic parameters (other than liquid diffusion) in a common matrix **K** that is defined by the specific problem, e.g., exchange and ET. In contrast to the analytical solution that requires appropriate simplifications, this numerical approach allows the full description of the influence of chemically induced magnetization transfer on any practical number of hyperfine (hf) lines. As the complete set of hf lines is considered, the important restriction of earlier analysis to the experimental parameters or the investigated system, namely, that the smallest separation of two hf lines must be larger than the microwave field strength, is removed. The limit is given by the computational facility. The effects of sequential radical reactions as well as chemical exchange on the time-dependent polarized EPR signal are illustrated in examples. TREPR spectra of laser flash induced semiquinones of *p*-benzoquinone are presented at two different pH values and solvents. The signals depending on magnetic field and time are found to exhibit effects caused by magnetization transfer, which results from different mechanisms. Their characteristic features are compared to the examples discussed. Computations obtained by the specified method are then

* Corresponding author. Telephone: (773) 702-7864. Fax: (773) 702-9646. E-mail: j-norris@uchicago.edu.

† Member of Institute for Biophysical Dynamics.

10.1021/jp0135149 CCC: $22.00
Published on Web 03/21/2002

presented and found in excellent agreement with the experiment. Finally, degenerate and nondegenerate proton exchange depending on the experimental conditions can be identified as illustrated by investigating *p*-benzosemiquinone with TREPR.

Theory

Under the conditions generally assumed for laser flash photolysis experiments, namely that the oscillating magnetic field strength ω_1 is smaller than the closest magnetic field separation of any two lines under consideration, that the initial polarization P_i is created before the observation starts, and that the magnetization transfer mechanisms are absent, the magnetization of a hyperfine (hf) line i, $M^i(t)$, is described by eq 1[3,4,6,20]

$$\frac{\mathrm{d}}{\mathrm{d}t}M^i(t) = \mathbf{L}^i M^i(t) + F^i(t) + \frac{(\mathrm{d}/\mathrm{d}t)n(t)}{n(t)}M^i(t) \qquad (1)$$

where

$$M^i(t) = \begin{pmatrix} M_x{}^i(t) \\ M_y{}^i(t) \\ M_z{}^i(t) \end{pmatrix}, \mathbf{L}^i = \begin{pmatrix} -\frac{1}{T_2{}^i} & \Delta\omega^i & 0 \\ -\Delta\omega^i & -\frac{1}{T_2{}^i} & \omega_1 \\ 0 & -\omega_1 & -\frac{1}{T_1{}^i} \end{pmatrix},$$

$$F^i(t) = \begin{pmatrix} 0 \\ 0 \\ 1 \end{pmatrix} P_{\mathrm{eq}}{}^i \frac{1}{T_1{}^i} n(t)$$

The radical concentration $n(t)$ is given by the appropriate rate law, P_{eq} denotes the equilibrium polarization, and T_1 and T_2 are the spin−lattice and spin−spin relaxation times. The offset from resonance is referred to as $\Delta\omega$. The third term on the right-hand side of eq 1 refers to the radical termination reaction that is assumed as a first-order reaction. The occurrence of magnetization transfer from hf lines k, l, m, ... can be accounted for by extending eq 1 to

$$\frac{\mathrm{d}}{\mathrm{d}t}M^i(t) = \mathbf{L}^i M(t) + F^i(t) + \frac{(\mathrm{d}/\mathrm{d}t)n(t)}{n(t)}M^i(t) - \alpha \mathrm{K}^i M^i(t) + \beta \mathrm{K}^k M^k(t) + \gamma \mathrm{K}^l M^l(t) + \ldots \qquad (2)$$

where the diagonal matrices **K** contain the quantities (exchange rates, line degeneracies, ...) defined by the specific problem under consideration. The integer coefficients α, β, γ, ... are determined by the pathways of magnetization transfer. As a spectrum results from a superposition of all hf lines, it is convenient to replace the individual vectors M^i, M^k, M^l, ..., F^i, F^k, F^l, ..., and the matrices $\mathbf{L}^i$, $\mathbf{L}^k$, $\mathbf{L}^l$, ..., $\mathbf{K}^i$, $\mathbf{K}^k$, $\mathbf{K}^l$ by new vectors and a supermatrix according to

$$\mu(t) = \begin{pmatrix} M^i(t) \\ M^k(t) \\ M^l(t) \\ \cdot \end{pmatrix}, \Phi(t) = \begin{pmatrix} F^i(t) \\ F^k(t) \\ F^l(t) \\ \cdot \end{pmatrix},$$

$$\mathbf{\Lambda} = \begin{pmatrix} \mathbf{L}^i - \alpha\mathbf{K}^i & \cdot & \cdot & \cdot \\ \cdot & \mathbf{L}^k - \beta\mathbf{K}^k & & \\ \cdot & & \mathbf{L}^l - \gamma\mathbf{K}^l & \\ \cdot & & & \cdot \end{pmatrix} \qquad (3)$$

The off-diagonal elements of $\mathbf{\Lambda}$ represent the magnetization transfer connecting the respective hf lines and are defined by inserting the **K** matrices as the appropriate elements. The validity of this approach requires that nuclear spin transitions proceed slower than the magnetization transfer and that the electron spin is conserved during electron transfer or secondary radical formation. Two illustrative examples will be given below. Substituting $\mu(t)$[6] by

$$\mu(t) = P(t)\, n(t) \qquad (4)$$

where

$$\frac{\mathrm{d}}{\mathrm{d}t}n(t) = \mathbf{K}'n(t) + n(0) \qquad (4')$$

and where $\mathbf{K}'$ is the rate matrix describing the chemical kinetics. Equation 4 leads to the time-independent vector

$$Q = \Phi(t)\, n(t)^{-1} \qquad (5)$$

and hence

$$\frac{\mathrm{d}}{\mathrm{d}t}P(t) = \mathbf{\Lambda}P(t) + Q \qquad (6)$$

Because we include all hyperfine lines, the restriction that the oscillating magnetic field strength ω_1 is smaller than the closest separation of two EPR lines can be dropped. Equation 6 is transformed into its eigenspace by the matrix **S** containing the eigenvectors of $\mathbf{\Lambda}$, according to

$$\mathbf{S}^{-1}\frac{\mathrm{d}}{\mathrm{d}t}P(t) = \mathbf{S}^{-1}\mathbf{\Lambda}\mathbf{S}^{-1}\mathbf{S}P(t) + \mathbf{S}^{-1}Q \qquad (7)$$

The subscript λ in the following shall denote a vector or matrix in the eigenbasis of $\mathbf{\Lambda}$. The transformation (7) yields

$$\frac{\mathrm{d}}{\mathrm{d}t}P_\lambda(t) = \mathbf{\Lambda}_\lambda P_\lambda(t) + Q_\lambda \qquad (8)$$

where $P_\lambda(t) = \mathbf{S}^{-1}P(t)$, $Q_\lambda = \mathbf{S}^{-1}Q$, and $\mathbf{\Lambda}_\lambda = \mathbf{S}^{1-}\mathbf{\Lambda}\mathbf{S}$.

Solutions to the system of linear differential equations are found by substituting $Y = \mathbf{\Lambda}_\lambda P_\lambda(t) + Q_\lambda$ such that the integration of

$$\frac{\mathrm{d}Y(t)}{Y(t)} = \mathbf{\Lambda}_\lambda\, \mathrm{d}t \qquad (9)$$

results in

$$Y(t) = Y(0)\exp(\mathbf{\Lambda}_\lambda t) \qquad (10)$$

Resubstitution leads to

$$P_\lambda(t) = (P_\lambda(0) + \mathbf{\Lambda}_\lambda{}^{-1}Q_\lambda)\exp(\mathbf{\Lambda}_\lambda t) - \mathbf{\Lambda}_\lambda{}^{-1}Q_\lambda \qquad (11)$$

Equation 11 is easily transformed back from the eigenspace into the rotating frame:

$$P(t) = \mathbf{S}P_\lambda(t) \qquad (12)$$

The time-dependent magnetization is given by multiplication of eq 12 with $n(t)$ as determined by eq 4′. The formalism to solve eq 6 can be used for eq 4′ as well.

As a consequence of the definitions, the transient signal corresponding to each of the hf lines i, k, l, ... is given by

$\mu_{3n-1}(t)$, $n = 1, 2, 3, ...$ The observed signal $M(t)$ results from the superposition of all $\mu_{3n-1}(t)$ according to eq 13 with respect to their Larmor frequency and the magnetic field position, which is taken into account by $\Delta\omega$.

$$M(t) = \sum_n \mu_{3n-1}(t) \tag{13}$$

Experimental Section

The spectrometer consists of a Varian E-Line based magnet and field controller, equipped with a personal computer for automation. The field is measured independently with a Bruker ER 035 M gaussmeter. A Bruker microwave bridge ER 041 MR has been modified to enhance time resolution and increase sensitivity. The raw signal is amplified with a Hewlett-Packard 461A and directed into a LeCroy 9450 oscilloscope. The data are stored in the personal computer. A Varian V-Line optical transmission cavity is attached to the microwave bridge. The samples were flowed through a Suprasil quartz flat cell. The flow rate was sufficiently fast that each laser flash excited fresh solution. A Lambda Physik excimer laser EMG 103 MSC, operated at $\lambda = 308$ nm, 20−100 Hz repetition rate, ∼10−20 mJ/ pulse at the sample, and 15−20 ns pulse width, serves as light source. Synchronization with the signal recorder is achieved via a fast photodiode. The EPR signal rise time was determined to be 20−30 ns.

Ethylene glycol, 2-propanol, and deuterium oxide were purchased from Fisher and used without further purification. Benzoquinone was obtained from Acros and purified according to standard methods[2] prior to use. Concentrations of benzoquinone were 18 and 9 mM for ethylene glycol and water/2-propanol samples.

Calculations were performed on a Dell Dimension personal computer (750 MHz) using the Compaq Visual Fortran 6.5.0 compiler or a Mathcad 2001 spreadsheet.

Results

We will now present two examples to illustrate the model:

1. Secondary radicals B, $a_B = 0$, are created from primary radicals A, $a_A = 0$ with an arbitrary g-value difference of $\Delta gB_0 = 0.4$ mT. It is also assumed that the radical lifetimes are much longer than the relaxation times. The appropriate 2×2 supermatrix describing the magnetization transfer in this particular case is given by

$$\mathbf{\Lambda} = \begin{pmatrix} \mathbf{L}^A - \mathbf{K}^A & \mathbf{0} \\ \mathbf{K}^A & \mathbf{L}^B - \mathbf{K}^B \end{pmatrix}, \mathbf{K}^x = k_x \cdot \mathbf{1}, x = \text{A, B} \tag{14}$$

where k_A is the reaction rate constant, $\mathbf{1}$ is the 3×3 identity matrix, and $\mathbf{0} = 0 \cdot \mathbf{1}$.

On-resonance transients of both signals are given in Figure 1 for three different sets of parameters as indicated in the legend. As can be readily recognized from the k-values, parts a and b of Figure 1 correspond to reactions

$$\text{A} \xrightarrow{k_A} \text{B} \tag{15}$$

and

$$\text{A} \underset{k_B}{\overset{k_A}{\rightleftharpoons}} \text{B} \tag{16}$$

respectively, with $k_A > k_B$. The sigmoidal rise, indicating a signal from a secondary species, is clearly seen. For comparison,

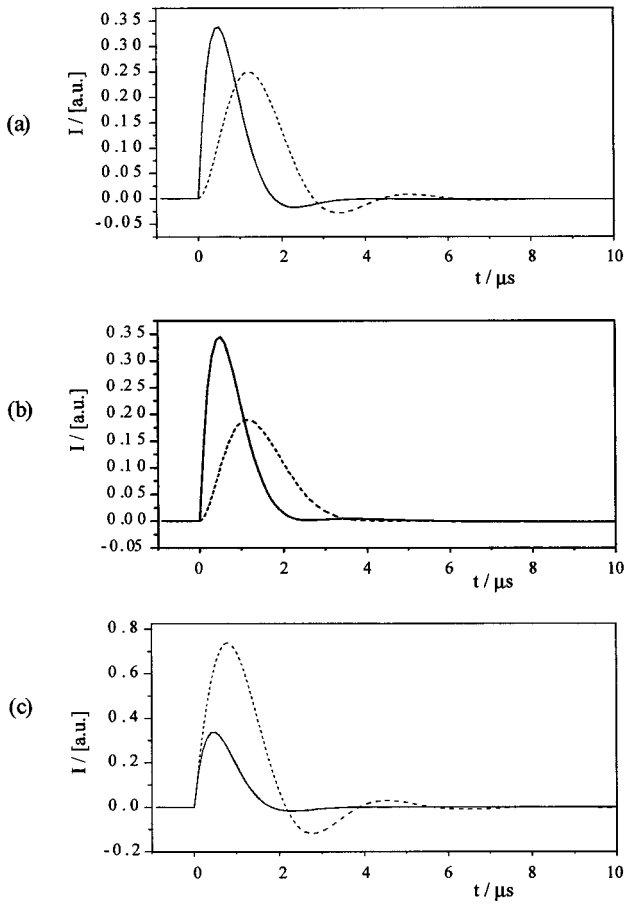

Figure 1. Calculated transient signals on-resonance assuming $T_{1A} = T_{1B} = 3$ μs, $T_{2A} = T_{2B} = 0.8$ μs, $a_A = a_B = 0$, $\Delta gB_0 = 0.4$ mT, $\omega_1 = 1.8$ rad MHz; species A is represented by the solid line, species B by the dashed line. Time traces correspond to reaction 15 with $k_A = 8.9 \times 10^5$ s^{-1}, $k_B = 3.6 \times 10^{-5}$ s^{-1} (a), to reaction 16 with $k_A = 8.9 \times 10^5$ s^{-1}, $k_B = 4.4 \times 10^5$ s^{-1} (b), and to reaction 17 with $k_A = 8.9 \times 10^5$ s^{-1}, $k_B = 3.6 \times 10^{-5}$ s^{-1} (c). Emission is arbitrarily set to positive values.

the signals caused by the reaction are shown in Figure 1c. The

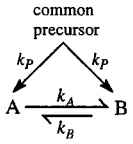

(17)

creation of A and B via k_P is assumed much faster than the time resolution of the detection method. As expected, both A and B now exhibit the pseudolinear rise in their transients, which is observed for primary radicals. However, the maximum of species B's signal is reached at later times as compared to that of species A.

2. Electron transfer occurs between two radicals with $a_A = 0$ of intensity 2, $a_B = 0.4$ mT, and $\Delta g = 0$. The matrix $\mathbf{\Lambda}$ now has the dimension 3×3:

$$\mathbf{\Lambda} = \begin{pmatrix} \mathbf{L}^B - \mathbf{K}^B & \mathbf{K}^A & \mathbf{0} \\ \mathbf{K}^B & \mathbf{L}^A - 2\mathbf{K}^A & \mathbf{K}^B \\ \mathbf{0} & \mathbf{K}^A & \mathbf{L}^B - \mathbf{K}^B \end{pmatrix}, \mathbf{K}^x = k_x \cdot \mathbf{1}, x = \text{A, B} \tag{18}$$

The essential features of electron transfer effects on TREPR spectra, when $\tau_A = \tau_B$, can be seen in the calculated signals presented in Figure 2: broadening of the 1:2:1 intensity

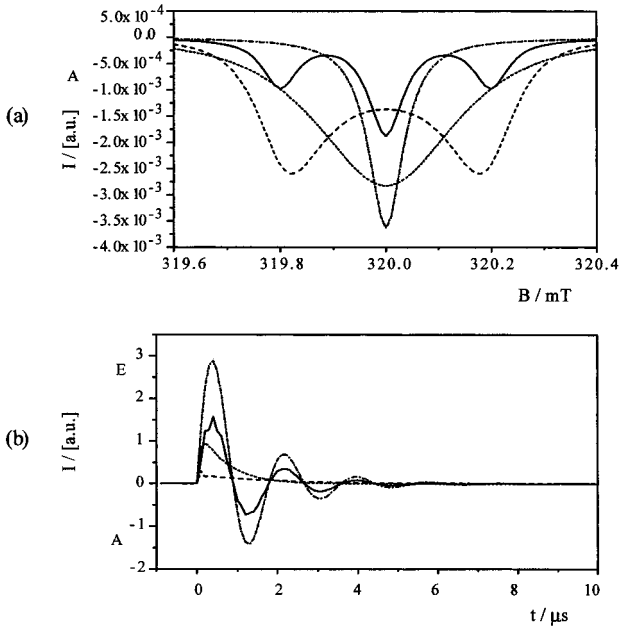

Figure 2. Calculated TREPR signals of electron transfer characterized by $T_{1A} = T_{1B} = 3\ \mu$s, $T_{2A} = T_{2B} = 0.8\ \mu$s, $a_A = 0$, $a_B = 0.4$ mT, $\Delta g = 0$, $\omega_1 = 3.5$ rad MHz; $\tau_A = \tau_B = 0.1$ s (solid line), $\tau_A = \tau_B = 0.1\ \mu$s (dashed line), $\tau_A = \tau_B = 0.05\ \mu$s (dotted line), $\tau_A = \tau_B = 10$ ps (dashed−dotted line); EPR spectrum (field representation) at 19 μs (a) after the laser flash; transients taken at center resonance (b). Emission is arbitrarily set to positive values.

distribution, shift of the line positions with increasing exchange, collapsing of the three hf lines into a single line, and line narrowing in the fast limit. The rather strong line broadening, even with no exchange, is due to the high microwave field strength, since oscillations in the field domain are no longer observed at times of about 19 μs. The corresponding transients, taken at the center resonance, are shown in Figure 2b. Signals with pure Torrey oscillations can only be observed in the limits of slow and fast exchange. The intermediate region exhibits fast oscillations that reflect the frequencies of the microwave field ω_1 and the separation from the neighboring lines.

It is also instructive to compare the combined relaxation and kinetic matrix for electron transfer, as in example 2, and an example for chemical exchange.

3. Interconversion leads to exchange of the hf splittings from two nuclei A and B with $I_A = I_B$ and $a_A \neq a_B$.

$$\mathbf{\Lambda} = \begin{pmatrix} \mathbf{L}-\mathbf{K} & \mathbf{0} & \mathbf{0} & \mathbf{0} \\ \mathbf{0} & \mathbf{L}^{A}-\mathbf{K} & \mathbf{K} & \mathbf{0} \\ \mathbf{0} & \mathbf{K} & \mathbf{L}^{B}-\mathbf{K} & \mathbf{0} \\ \mathbf{0} & \mathbf{0} & \mathbf{0} & \mathbf{L}-\mathbf{K} \end{pmatrix}, \mathbf{K} = k\cdot\mathbf{1} \qquad (19)$$

Because of the degeneracy of the two interconverting species, the dimension of $\mathbf{\Lambda}$ can be reduced to 4×4. Completing the matrix to its 8×8 representation, where each hyperfine state of both species is fully considered, would allow treatment of nondegenerate exchange. Comparison of eqs 18 and 19 quickly exhibits the main differences between line width alteration due to ET and chemical exchange. While ET leads to equilibration of the populations of all hf lines, chemical exchange connects selected nuclear spin states characteristic of the nature of the magnetization transfer and thus of the chemistry.

When investigated by TREPR, the light-induced signals of *p*-benzoquinone are very sensitive to the conditions (solvent, pH, viscosity, purity, etc.) chosen. Signals obtained at pH 2 and 6.4 in a 1:1 mixture of water and 2-propanol are presented in parts a and b, respectively, of Figure 3 . While in the low pH region chemical exchange broadened hf lines are obvious, a superposition of the neutral and the anionic semiquinone is detected. A spectrum taken in ethylene glycol exhibits the neutral radical with traces of the anion.[7,10,21] On monitoring the time domain at various magnetic fields that correspond to the arrows in the frequency representation, cf. Figure 3c−e, the transients are found to reflect the effects of different types of magnetization transfer. Therefore, to achieve very good agreement between experimental and calculated EPR signals, common hf coupling constants (as given in Table 1) are used for the computation, but different magnetization transfer rates are required. For the exchange-broadened spectrum in Figure 3a and the selected time trace in Figure 3c, proton transfer between two neutral semiquinones with a rate of 1.85×10^7 s^{-1} is assumed. The calculated spectrum is shown in Figure 3a (bottom) and the transient in Figure 3c. The time-dependent signal of the neutral semquinone observed at pH 6.4 reveals that the superimposed signals of neutral and anion radicals are nonetheless related by proton transfer. The rates are evaluated to be 3.9×10^5 s^{-1} for the deprotonation and 3.3×10^5 s^{-1} for the protonation reaction. This exchange is not easily recognized in the frequency domain. Calculated signals are again presented in Figure 3b (bottom) and 3d. Even larger differences in the rate constants of the magnetization transfer are observed for the semiquinone in ethylene glycol, which cannot be identified from a single field domain spectrum. The experimental curve of the on-resonance magnetization of the first high field hf line is presented in Figure 3e. The simulation can be best accommodated by assuming a fast deprotonation from the neutral semiquinone to the anionic semiquinone species with a rate of 2.0×10^6 s^{-1}. Protonation of the semiquinone anion proceeds with a rate of 2.5×10^5 s^{-1}. The reaction is described by modifying eq 17, where k_P is much faster than the time resolution of the spectrometer. The calculated time profile is given in Figure 3e as well.

Discussion

Using a personal computer with a compiled Fortran program, numerical solutions are computed as fast as seconds up to a few minutes for exchange involving 3−30 hf lines. As might be expected, the most time-consuming step is the computations of the eigenvalues and eigenvectors of $\mathbf{\Lambda}$. The parameters characteristic of the chemical process that induces magnetization transfer are included in a single algorithm. Hence, different phenomena such as chemical exchange or sequential chemical reactions can be analyzed in the same way as demonstrated by the examples in Figures 1 and 2. The influences of the mechanisms on the time development of the magnetization can be directly visualized by comparison of the specific kinetic matrices. Nevertheless, although no analytical solution is obtained or could even be obtained for the general case, still the possibility exists to decompose the signal at a given magnetic field into its contributions from the individual hf lines using eq 13. The fact that in principle every system that exhibits the phenomena of magnetization transfer can be treated by considering each of the hf states separately while simultaneously finding the kinetic matrix is likely the greatest advantage of the method. No simplification to reduce the dimension of the problem suitable for analytical solutions needs to be sought in view of the speed of today's personal computers. The complexity of the system under consideration is only limited by the capacity of the computer used and the time required for the calculation.

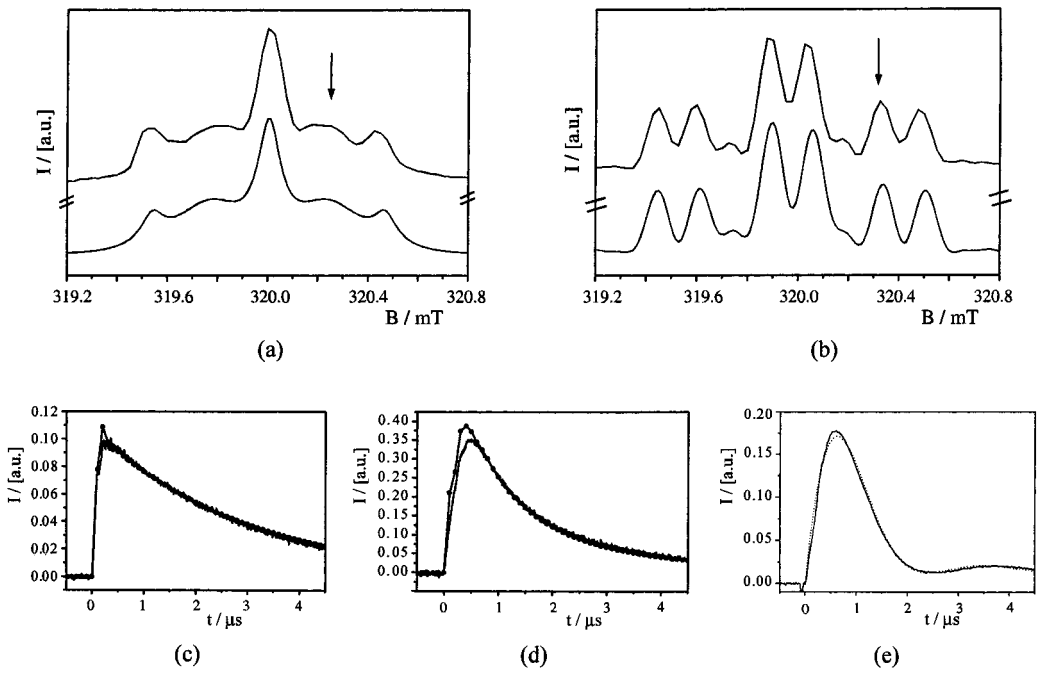

Figure 3. TREPR spectra of BQ (9 mM) in water:2-propanol 1:1 320 ns after the laser flash, pH 2 (a), pH 7.3 (b); experimental spectra shown on top, calculated at the bottom. Transient signals are recorded at the following magnetic fields: first high-field resonance of the exchange spectrum in (a) indicated by the arrow (c); second high-field resonance in (b) as indicated (d); second high-field line of $BQH^{\bullet}$ (18 mM) in ethylene glycol (e); experimental signals are represented by solid lines, calculated ones by dotted lines. Emission is arbitrarily set to positive values.

TABLE 1: Hyperfine Coupling Constants *a*, Relaxation Times *T*, Magnetic Field Strength ω_1, and Magnetization Transfer Rates for the Neutral and Anionic Benzosemiquinone ($BQH^{\bullet}$ and $BQ^{\bullet-}$)

		solvent		
radical species	*a*/mT	pH 2, 2-propanol−H_2O	pH 7.3, 2-propanol−H_2O	ethylene glycol
$BQH^{\bullet}$	2 H(*o*-H): 0.450 2 H(*m*-H): 0.017 H(OH): 0.170	$k_{H^+} = 1.85 \times 10^7\ s^{-1}$	$k_{-H^+} = 3.90 \times 10^5\ s^{-1}$	$k_{-H^+} = 2.0 \times 10^6\ s^{-1}$
$BQ^{\bullet-}$	4 H(ar): 0.225		$k_{+H^+} = 3.30 \times 10^5\ s^{-1}$	$k_{+H^+} = 2.5 \times 10^5\ s^{-1}$
$BQH^{\bullet}$ and $BQ^{\bullet-}$		$T_1 = 5.0\ \mu s$ $T_2 = 1.0\ \mu s$ $\omega_1 = 1.76$ rad MHz	$T_1 = 3.0\ \mu s$ $T_2 = 0.35\ \mu s$ $\omega_1 = 0.88$ rad MHz	$T_1 = 5.0\ \mu s$ $T_2 = 0.70\ \mu s$ $\omega_1 = 1.93$ rad MHz

The examples chosen in eqs 15−17, together with the characteristic matrices $\mathbf{\Lambda}$ in eqs 14, 18, and 19, provide a selection of various magnetization transfer processes. They greatly complicate the signal that otherwise would be determined solely by the simple Bloch equations. However, it is easily visualized by looking at the corresponding $\mathbf{\Lambda}$ that such different phenomena as secondary radical creation and proton transfer may have the same effect on the TREPR signal especially in the time domain, depending on the hf states involved. Figure 1 demonstrates the effects of exchange depending on time, which reflect the kinetic aspects of the assumed chemistry. In contrast, the nature of the phenomenon is often better recognized in the frequency domain, cf. Figure 2a. For example, the transient signals in Figure 2b at the highest and lowest exchange rate impart strong Torrey oscillations with no obvious decay other than the relaxation times. Hence, no easy initial guess exists concerning their relative rate of exchange. In contrast, a frequency domain spectrum readily reveals the qualitative range of exchange, i.e., slow, coalescence, or fast, but does not allow quantification without the help of a series of spectra at various magnetization transfer rates. While proton transfer tends to connect hf states selectively, electron transfer equilibrates spin populations independent of selection rules. This is reflected in the kinetic matrices of eqs 18 and 19. Hence, in the case of ET, line broadening may be observed for all hf lines, their decay time depending on the line degeneracy, whereas for proton exchange, alternating line width effects are very common.[1,27]

Within the computed examples, the radical termination reactions are chosen much longer than the relaxation times, as is generally the case in laser flash photolysis TREPR experiments. Nevertheless, the chemical lifetime of the radicals can also be accounted for by choosing the appropriate rate laws for $n(t)$ in eq 4′.

In praxis, it is convenient to rely on the complete signal surface as a function of time and magnetic field, as more than one exchange mechanism might be present in the system. As discussed above, the TREPR study of BQ provides an instructive example of chemical exchange that demonstrates magnetization transfer. The broadening of the hf components, i.e., the second and fourth lines of a five-line spectrum, has been reported for the steady-state EPR spectrum.[22,28] The assumption of an intermolecular proton exchange, connecting the hf states of two neutral semiquinones and characterized by $k_{H^+} = 1.85 \times 10^7\ s^{-1}$, leads to excellent agreement between experiment and calculation, cf. Figure 3a,c. The estimated rate constant is found to be very close to that determined earlier[22] even though the latter is based on the proposed exchange between the neutral and the anionic semiquinone. While the frequency-dependent spectrum can be simulated using either mechanism, we nevertheless favor the degenerate exchange mechanism because the

time-dependent signals show better agreement compared to nondegenerate exchange. In consequence, intermolecular proton transfer equilibrium is assumed. When raising the pH to about neutral, the coexistence of the anionic and neutral species is clearly recognized in the time-resolved frequency spectra. Still a slow proton transfer exists between both forms of the semiquinone, which is indicated by the time domain decay curves. The deprotonation rate $k_{-H^+} = 3.90 \times 10^5\ s^{-1}$ is slightly higher than the protonation reaction, being $k_{+H^+} = 3.30 \times 10^5\ s^{-1}$. It has to be mentioned that no $BQH^\bullet$ is detected in the steady-state EPR spectra at both pH values. The three-dimensional TREPR spectrum can be well simulated according to the scheme in eq 17. A value for the formation rate of $BQH^\bullet$ or $BQ^{\bullet-}$ cannot be estimated due to the time resolution of the observation, but the signal intensities indicate the predominant formation of $BQH^\bullet$ compared to $BQ^{\bullet-}$. The slower protonation rate reflects the greater thermodynamic stability of the anion at this pH, which is detected as the only species in the equilibrated spectrum. In ethylene glycol, the discrepancy in the protonation and deprotonation rate is found to be even higher. The kinetic scheme still follows eq 17. The rate constant amounts to $k_{-H^+} = 2.0 \times 10^6\ s^{-1}$. The protonation then proceeds slower, or less frequently, by a factor of about 10 with $k_{+H^+} = 2.5 \times 10^5\ s^{-1}$. As was the case at pH 6.4, the neutral semiquinone is predominantly formed from the common precursor state. The rate constants reflect the much weaker acidity of ethylene glycol versus $BQH^\bullet$ and hence render the protonation more rare. Again, protonation and deprotonation are of intermolecular origin. While the exchange in the magnetic field domain is barely recognized, the identification of chemical exchange can readily be achieved by means of the transient signals.

In summary, ESP transfer at higher rates is readily recognized in the field domain often by dramatic line width effects, whereas observing the time dependence of the signal better reveals slow processes. In particular, damping of Torrey oscillations at higher microwave fields, which corresponds to an apparent shortening of T_2, i.e., the observation of an effective T_2, is indicative for magnetization transfer.

Conclusion

For the solution of the Bloch equations extended to include magnetization transfer, a computational treatment via reduction to an eigenvalue/eigenvector problem is discussed. By combining the matrix containing the magnetic resonance specific parameters, such as magnetic field, relaxation times, and microwave field strength, with the kinetic matrix characteristic to the magnetization transfer mechanism, a complete description of TREPR signals is achieved without the need for reduction of the system's dimensionality. The effects of electron transfer, proton transfer, and secondary radical generation on the magnetization in the time and field domains are illustrated. While strong line broadening is readily recognized in the frequency spectrum, the time domain provides easy access to the quantitative analysis of the phenomenon under consideration. However, a single transient does not elucidate the nature of the magnetization transfer mechanism as it only reflects the rate constants. On the other hand, the spectrum might be interpreted in terms of electron transfer or proton exchange, especially when no specific alternating line width effects are present.

The computational algorithm is successfully applied to the laser-generated CIDEP TREPR signals of *p*-benzosemiquinones in aqueous 2-propanol as well as in ethylene glycol. Significant proton exchange was found in these solvents. At pH 2, the TREPR spectra are interpreted in terms of a fast intermolecular proton exchange between neutral semiquinones. Raising the pH to 6.4 not only decreases the exchange rate but also alters the exchange process, which now proceeds between the anionic and the neutral radical of benzoquinone. From a common precursor, $BQH^\bullet$ is formed preferentially but the anion is the more stable species under the experimental conditions. For BQ in ethylene glycol, spectral analysis reveals a fast deprotonation leading from $BQH^\bullet$ to $BQ^{\bullet-}$, and a slow intermolecular protonation reaction transforming the anion back to the neutral species.

Acknowledgment. M.J. and J.R.N. acknowledge support from the U.S. Department of Energy, Office of Basic Energy Sciences, and Division of Chemical Sciences Contract No. DE-FG02-96ER14675. M.J. is especially thankful for a Feodor Lynen Fellowship from the Alexander von Humboldt Foundation.

References and Notes

(1) Carrington, A.; McLachlan, A. D. *Introduction to Magnetic Resonance With Applications to Chemistry and Chemical Physics*, 1st ed.; Harper & Row: New York, Evanston, and London, 1967.

(2) Craw, M. T.; Depew, M. C.; Wan, J. K. S. *Can. J. Chem.* **1986**, *64*, 1414−1417.

(3) Eastman, M. P.; Kooser, R. G.; Das, M. R.; Freed, J. H. *J. Chem. Phys.* **1969**, *51*, 2690−2709.

(4) Freed, J. H. *J. Phys. Chem.* **1967**, *71*, 38−51.

(5) Hore, P. J.; Joslin, C. G.; McLauchlan, K. A. *Chem. Soc. Spec. Per. Rep. ESR* **1979**, *5*, 1−45.

(6) Hore, P. J.; McLauchlan, K. A. *Mol. Phys.* **1981**, *42*, 533−550.

(7) Jäger, M.; Norris, J. R., Jr. *J. Magn. Reson.* **2001**, *150*, 26−34.

(8) Jockusch, S.; Liu, Z.; Ottaviani, M. F.; Turro, N. J. *J. Phys. Chem. B* **2001**, *105*, 7477−7481.

(9) Koptyug, I. V.; Goloshevsky, A. G.; Zavarine, I. S.; Turro, N. J.; Krusic, P. J. *J. Phys. Chem. A* **2000**, *104*, 5726−5731.

(10) Lendzian, F.; Jaegermann, P.; Moebius, K. *Chem. Phys. Lett.* **1985**, *120*, 195−200.

(11) Li, G.; Mu, J.; Li, X.; Lu, T.; Sun, W. *Colloids Surf., A* **2001**, *182*, 269−274.

(12) McCaffrey, V. P.; Forbes, M. D. E. *Tetrahedron* **2000**, *56*, 6991−6997.

(13) McLauchlan, K. A. *J. Chem. Soc., Perkin Trans. 2* **1997**, 2465−2472.

(14) McLauchlan, K. A.; Ritchie, A. J. D. *Mol. Phys.* **1985**, *56*, 1357−1367.

(15) McLauchlan, K. A.; Ritchie, A. J. D. *Mol. Phys.* **1985**, *56*, 141−159.

(16) McLauchlan, K. A.; Yeung, M. T. *Mol. Phys.* **1996**, *89*, 1423−1443.

(17) Monchik, L.; Adrian, F. J. *J. Chem. Phys.* **1978**, *68*, 4376−4383.

(18) *Chemically Induced Magnetic Polarization*; Muus, L. T., Atkins, P. W., McLauchlan, K. A., Pedersen, J. B., Eds.; D. Reidel: Dordrecht, 1977.

(19) Nishioku, Y.; Ohara, K.; Mukai, K.; Nagaoka, S.-i. *J. Phys. Chem. B* **2001**, *105*, 5032−5038.

(20) Pedersen, J. B. *J. Chem. Phys.* **1973**, *59*, 2656−2667.

(21) Pedersen, J. B.; Hansen, C. E. M.; Parbo, H.; Muus, L. T. *J. Chem. Phys.* **1975**, *63*, 2398−2405.

(22) Smith, I. C. P.; Carrington, A. *Mol. Phys.* **1967**, *12*, 439−448.

(23) Takamori, D.; Aoki, T.; Yashiro, H.; Murai, H. *J. Phys. Chem. A* **2001**, *105*, 6001−6007.

(24) Torrey, H. C. *Phys. Rev.* **1949**, *76*, 1059−1068.

(25) Verma, N. C.; Fessenden, R. W. *J. Chem. Phys.* **1976**, *65*, 2139−55.

(26) Weissman, S. I. *Annu. Rev. Phys. Chem.* **1982**, *33*, 301−318.

(27) Wertz, J. E.; Bolton, J. R. *Electron Spin Resonance: Elementary Theory and Practical Applications*, 1st ed.; McGraw-Hill: New York, 1972.

(28) Yamazaki, I.; Piette, L. H. *J. Am. Chem. Soc.* **1965**, *87*, 986−990.